ACS APPLIED MATERIALS & INTERFACES

Research Article

www.acsami.org

Functionalized Mesoporous Silica Nanoparticles with Redox-Responsive Short-Chain Gatekeepers for Agrochemical Delivery

Zhifeng Yi,[†] Hashmath I. Hussain,[‡] Chunfang Feng,[†] Dequan Sun,[‡] Fenghua She,[†] James E. Rookes,[‡] David M. Cahill,*[,‡] and Lingxue Kong*[,†]

[†]Institute for Frontier Materials, Deakin University, Geelong Campus at Waurn Ponds, Geelong, Victoria 3216, Australia

[‡]Center for Chemistry and Biotechnology, School of Life and Environmental Sciences, Deakin University, Geelong Campus at Waurn Ponds, Geelong, Victoria 3216, Australia

Supporting Information

ABSTRACT: The controlled release of salicylic acid (SA), a key phytohormone, was mediated by using a novel decanethiol gatekeeper system grafted onto mesoporous silica nanoparticles (MSNs). The decanethiol was conjugated only to the external surfaces of the MSNs through glutathione (GSH)-cleavable disulfide linkages and the introduction of a process to assemble gatekeepers only on the outer surface so that the mesopore area can be maintained for high cargo loading. Raman and nitrogen sorption isotherm analyses confirmed the successful linkage of decanethiol to the surface of MSNs. The *in vitro* release of SA from decanethiol gated MSNs indicated that the release rate of SA in an environment with a certain amount of GSH was significantly higher than that without GSH. More importantly, *in planta* experiments showed the release of SA from decanethiol gated MSNs by GSH induced sustained expression of the plant defense gene *PR-1* up to 7 days after introduction, while free SA caused an early peak in *PR-1* expression which steadily decreased after 3 days. This study demonstrates the redox-responsive release of a phytohormone *in vitro* and also indicates the potential use of MSNs *in planta* as a controlled agrochemical delivery system.

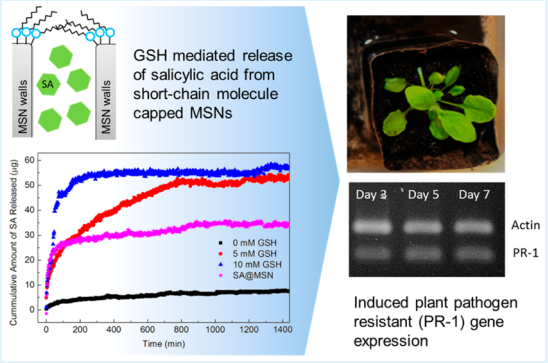

KEYWORDS: *mesoporous silica nanoparticles (MSNs), stimuli-response, redox-responsive gatekeepers, decanethiol gatekeepers, agrochemical delivery system*

1. INTRODUCTION

Nanoparticles made of gold, semiconductor nanocrystals, super-paramagnetic, silicon, and silica-based materials have been extensively studied as promising candidates for drug delivery. Among these inorganic-based particles, mesoporous silica nanoparticles (MSNs) are particularly attractive in potential applications as a biomolecule carrier, due to the favorable properties such as high surface area and porosity,[1,2] controllable particle and pore sizes,[3−6] versatile surface functionalization,[7−9] and low toxicity to both animals and plants.[10−13] The controlled drug delivery system using functionalized MSNs has been well-developed to deliver anticancer drugs or silencing nucleotides into various mammalian cells and tissues.[11,14−16] The recent studies in plant science have focused on the delivery of MSNs loaded with large molecules such as proteins and DNA by the gene gun or ultrasound to penetrate the cell wall barriers, which indicates the potential of using MSNs in plants.[17−19] However, the use of MSNs as a controlled delivery vehicle for agricultural applications is yet to be reported as the cell wall prevents the uptake of MSNs by plants and the translocation of MSNs within plants.

The use of appropriate gatekeepers on mesoporous nanoparticles can release biomolecules in a controllable fashion. The gatekeeper acts as a blocking component at the entrance of the pores of the nanoparticles. Gatekeepers can be designed to enable MSNs to release cargos in response to trigger factors such as pH,[20−23] temperature,[24] light[25−27] and redox mediators.[28−30] Among these factors, redox-responsive gatekeepers are advantageous due to the fact that the endogenous reductants such as glutathione in cells can be utilized to open gatekeepers without exogenous agents. Several redox-responsive gatekeeper systems have been developed, such as gold nanoparticles,[19] cadmium sulfide (CdS),[31] magnetic nanoparticles (Fe_3O_4),[32] β-cyclodextrins[30,33] and thiol-terminated poly(ethylene glycol) (PEG-SH)[29] for mammalian systems. However, the drawbacks of these gatekeepers limit their applications in plant systems. The use of heavy metal particles in plants always presents safety issues,[34] as the accumulated heavy metals in plants may in turn lead to side effects on

Received: March 10, 2015
Accepted: April 22, 2015
Published: April 22, 2015

DOI: 10.1021/acsami.5b02131
ACS Appl. Mater. Interfaces 2015, 7, 9937−9946

herbivores or human beings. The control of the size of MSNs within a certain range is essential for the translocation in plants.[34] The use of gold or magnetic particles or PEG-SH coating to manipulate the drug release could enlarge the particle size, leading to the deteriorative transportation of MSNs within plants. Although the β-cyclodextrin gatekeepers reported in recent studies minimize the size effects before and after the encapsulation of biomolecules,[30,33] the effects of cyclodextrins on plants are controversial and inconclusive,[35] as an inhibition of plant growth and an increased growth were observed in the presence of cyclodextrins and after cyclodextrins were metabolized, respectively.[35] Moreover, the cyclodextrin gatekeeper system released cargos very quickly from smaller nanoparticles even at a very low GSH concentration,[30,33] which was not ideal for the agrochemical delivery system that required sustained release.[36] Therefore, a new design of gatekeepers is required to safely deliver agrochemicals into plants and maintain the transporting ability of MSNs.

The redox-responsive release of biomolecules triggers when the disulfide bonds formed between MSNs and gatekeepers are cleaved by GSH, a protein naturally existing in both plant and animal cells. Once the gatekeepers are removed from the pore entrance, the loaded molecules can freely diffuse into the cells and conduct their function within cells.[30] So far, the feasibility to release cargos into plants in a redox-responsive fashion has been proved in the protoplast that is the plant cell with the cell wall chemically removed.[19] However, there is no report about the application of redox-responsive gatekeepers in intact plants.

Furthermore, particle size plays an important role in the penetration and translocation of particles in plants. Plant cell walls have pores of a size between 5 and 30 nm,[37−41] which are the most probable pathway for nanoparticles to enter plant cells. A recent study showed the accumulation of MSNs with the diameter of about 50 nm in the roots of intact plants, but no MSNs in the shoot system was observed,[42] which means that the size of the MSNs limits their translocation within plants. As shown in previous studies, nanoparticles with the particle size of 20 nm or less can transport through plant cells and reach the shoot system.[34] Our previous studies[12,43] have also indicated that MSNs with a particle size of ∼20 nm can be taken up by intact plants and transported through the root system to the shoot system but have no impacts on seed germination and plant growth in various plant species such as *Arabidopsis*, wheat, and lupin. Therefore, the small particle size (∼20 nm) offers good permeability through plant cell walls and benefits the translocation of MSNs within plants.

This work aims to demonstrate the possibility of using redox-responsive gatekeepers to control the delivery of biomolecules into intact plants. The well-dispersed MSNs with a particle size of about 20 nm were fabricated and a redox-responsive short-chain molecular gatekeeper was introduced to control the release of a model plant hormone in plants. The gatekeepers were assembled onto MSNs with a localized functionalization but without significant changes in particle size and can be opened by GSH-mediated cleavage of disulfide bonds. This study shows the rationale of gatekeeper assembly, controlled release *in vitro* and *in vivo*, and demonstrates its potential application in agriculture.

2. EXPERIMENTAL SECTION

2.1. Materials. Cetyltrimethylammonium bromide (CTAB, ≥99%), tetraethyl orthosilicate (TEOS, 98%), 3-mercaptopropyltrimethoxysilane (MPTMS), decanethiol (96%), sodium iodide (99.5%), glutathione reduced (GSH, ≥98%), and salicylic acid (SA, >99%) were purchased from Sigma-Aldrich. Ammonium hydroxide (30 wt %), ethyl acetate, sodium carbonate, hydrogen peroxide solution (30 wt %), absolute ethanol, and hydrochloric acid (32 wt %) were all AR grade. All of the chemicals were used without further purification.

2.2. Synthesis of Mesoporous Silica Nanoparticles. The MSNs were synthesized by using CTAB as a template to generate a silica mesoporous structure.[44−46] Specifically, 2.96 g of CTAB was dissolved in 100 mL of Milli-Q water with its pH being adjusted to 10 using ammonium hydroxide. The mixture was heated to and remained at 80 °C while stirring for 30 min in order to stabilize the structure of CTAB micelles. Subsequently, the aqueous CTAB solution was cooled to 30 °C followed by the dropwise addition of 1.86 mL of TEOS. The reaction was maintained for 24 h under a stirring speed of 550 rpm, followed by aging the mixture at 80 °C for 24 h. The products were filtered through an Anopore membrane with a pore size of 100 nm (Whatman) and washed with ethanol for several times to remove the free CTAB and TEOS. Finally, MSNs with CTAB that remained in the nanoparticles (CTAB@MSNs) were collected and dried under vacuum for further use. For comparison, MSNs that had the template CTAB removed were obtained by heating CTAB@MSNs at 600 °C for 5 h. The MSNs without the templates were collected after cooling to room temperature.

2.3. Grafting of Thiol Groups on CTAB@MSNs. Thiol (-SH) groups were then grafted onto the surface of the MSNs that contained the template CTAB to allow the functional groups to be implanted only at the entrance of mesopores. In detail, 100 mg of CTAB@MSNs was dispersed into 100 mL of absolute ethanol and the mixture was sonicated until a uniform suspension was achieved. Under vigorous stirring, 100 μL of MPTMS was added dropwise into the mixture. After 1 h, 1 mL of deionized water was added and the reaction was maintained for 24 h under room temperature with stirring. Then the mixture was heated to 80 °C to stabilize the silanol groups between MSNs and MPTMS. The products were centrifuged and washed with absolute ethanol for 3 times. Then the as-made CTAB@MSNs that were grafted with thiol were re-dispersed in a solution of 100 mL of absolute ethanol and 1 mL of hydrochloric acid (32%), and the mixture was stirred at 60 °C overnight to remove the CTAB inside the mesopores. The MSNs with CTAB template removed and modified with thiol were centrifuged in 50 mL centrifuge tubes at 8000 rpm for 7 min, washed with absolute ethanol for 3 times, and dried under vacuum at room temperature. Thiol-functionalized MSNs were denoted as MSN-SH.

2.4. Synthesis of Didecyl Disulfide. The disulfide bonds between thiols were formed through a mild oxidation procedure.[47] Specifically, 0.8 mL of decanethiol was dissolved in 12 mL of ethyl acetate under stirring. A 6 mg amount of sodium iodide and 0.44 mL of hydrogen peroxide (30 wt %) were added to the mixture. After stirring for 30 min at room temperature, the as-synthesized didecyl disulfide was washed by sodium carbonate aqueous solution (10 wt %) three times to remove abundant iodine and hydrogen peroxide. The final transparent oil-like product was collected by evaporating ethyl acetate in silica gel under room temperature.

2.5. Synthesis of Thiol-Capped MSNs. The previously synthesized didecyl disulfide was introduced to form gatekeepers at the entrance of mesopores. The procedures were as follows: 10 mg of template-removed MSN-SH was dispersed in 10 mL of ethyl acetate followed by addition of 25 μL of didecyl disulfide. The mixture was sonicated for 1 h and stirred for 24 h at room temperature. The capped MSN-SH (MSN-SS-C_{10}) was washed and centrifuged with ethyl acetate three times and absolute ethanol three times. Powders were collected by vacuum drying.

2.6. Loading of Salicylic Acid and Assembly of Decanethiol onto MSN-SH. The loading of salicylic acid (SA) was conducted through free diffusion. In details, 100 mg of SA was dissolved in 5 mL of ethyl acetate. Then, 100 mg of MSN-SH was added into the SA solution and the mixture was sonicated for 30 min. After shaking at room temperature for 24 h, 250 μL of didecyl disulfide was added to the mixture to react with -SH groups on MSN-SH. The reaction was

DOI: 10.1021/acsami.5b02131
ACS Appl. Mater. Interfaces 2015, 7, 9937−9946

maintained for 24 h with shaking on a rotating mixer at room temperature. Finally, SA-loaded and decanethiol-capped MSNs were centrifuged at 7500 rpm for 10 min and washed with 40% (v/v) ethanol once to remove most of the ethyl acetate. All of the supernatant was collected to measure the loading percentage of SA. MSN samples were quickly frozen in liquid nitrogen to keep the SA in the mesopores and then dried in a freeze-dryer for 24 h. The dried powder was collected for further use and denoted as SA@MSN-SS-C_{10}. The control samples loaded with SA but without any functionalization of the MSNs were also prepared using the same loading procedures and concentration. The loading was maintained for 48 h. This sample was denoted as SA@MSN.

2.7. Characterization. Transmission electron microscopy (TEM) images were obtained on a JEM-2100 electron microscope (JEOL, Tokyo, Japan) operating at an accelerating voltage of 200 kV. The suspension of MSN powder was dropped onto a copper grid with carbon film. Scanning electron microscopy (SEM) images were captured on a Supra 55VP (Zeiss, Oberkochen, Germany). All samples were coated with carbon using a BAL-TEC SCD 050 sputter coater (Leica Microsystems, North Ryde, Australia). The SEM energy dispersive spectra (SEM-EDS) were obtained from an X-Max 20 mm^2 SDD energy dispersive X-ray detector (Oxford, Abingdon, U.K.) in SEM. The data acquisition time was 10 min for mapping elements. Nitrogen adsorption−desorption isotherms were carried out on a Micromeritics Tristar 3000 analyzer (Particle & Surface Science, Dunstable, U.K.) at 77 K under a continuous adsorption condition. Prior to measurement, all samples were degassed at 40 °C for 24 h in a vacuum oven before measurement. The pore size distribution was calculated from adsorption branches of isotherms by the Barrett−Joyner−Halenda (BJH) method. Pore volume and specific surface area were calculated by using Brunauer−Emmett−Teller and Barrett−Joyner−Halenda (BET-BJH) methods. Thermogravimetric analysis (TGA) was conducted on a Netzsch STA 409 instrument (Seib, Germany) over a range of temperature from 60 to 700 °C at a rate of 15 °C/min under air atmosphere. Raman spectra were obtained by an inVia Raman microscope (Renishaw, Wolton-under-Edge, U.K.) at the laser wavelength of 514 nm. The ultraviolet visible spectra were obtained from USB-2000 and USB-4000 spectrometer (Ocean Optics, Dunedin, FL, USA).

2.8. *In Vitro* Releasing of Salicylic Acid. To investigate the effectiveness of the gatekeepers *in vitro*, SA-loaded MSNs and decanethiol-capped and SA-loaded MSNs were statistically tested under different concentrations of GSH. Ultraviolet visible spectrum was introduced to determine the amount of SA released from MSN samples. Specifically, 3 mg of MSN samples was placed on the top of a cuvette and the liquid in the cuvette was separated by a piece of dialysis tube in order to prevent the nanoparticles from moving to the bottom of the cuvette. The signal was collected from the bottom of the cuvette every 1 min. The liquid (3.5 mL) in the cuvette consisted of water and different concentrations of GSH (0, 5, and 10 mM). For comparison, the release of SA from nonfunctionalized MSNs using the same procedures and concentrations was also examined. The final release curve was averaged from three duplicates.

2.9. Plant Material and Growth Conditions. *Arabidopsis thaliana* (*A. thaliana*) ecotype Columbia-0 (Col-0) wild-type plants were obtained from the *Arabidopsis* Stock Center (Columbus, OH, USA). Seed accessions of Col-0 can be obtained from the *Arabidopsis* Stock Center (http://arabidopsis.info). A preliminary experiment was conducted to identify the prolonged expression of *PR1* gene to exogenous and MSNs loaded with SA and capped with decanethiol gatekeepers. The plants were grown with slight modification for further experiments.[48] The seeds were surface sterilized for 5 min with a solution containing 45% (v/v) sterile distilled water, 50% (v/v) ethanol, and 1.5% (v/v) hydrogen peroxide. The sterilization solution was removed, and the *Arabidopsis* seeds were rinsed three times with sterile distilled water to remove the residual sterilization solution. The seeds were then transferred to the plates containing the MS medium. The plates were sealed with parafilm and seeds were vernalized at 4 °C to improve and synchronize seed germination. The plates were then transferred to a plant growth chamber where seedlings were grown under controlled conditions (Thermoline, Coburg North, Australia) at 21 °C with a 16 h light (light intensity, 100 μmol m^{-2} s^{-1}) and 8 h dark cycle for 2 weeks. Small black pots were filled with fresh propagation mix (Debco, Tyabb, Australia), and the pots were placed in a plastic tray containing tap water. The soil on the surface of each pot was moistened with tap water from a squeeze bottle, and single holes were then made within the soil of each pot. *Arabidopsis* seedlings were gently removed from the MS media with forceps and care was taken to avoid any root damage. The seedlings were put into the hole and surrounded by soil. The tray containing the seedlings was covered with a clear transparent lid on top of the pots to minimize wilting during acclimatization. The seedlings were allowed to grow for 1 week and were further used for downstream applications.

2.10. Vacuum Infiltration of SA, MSNs, and SA@MSN-SS-C10. Three week old *Arabidopsis* seedlings were carefully removed from the pot, and the roots were washed gently in a tray containing tap water with repeated dipping to remove any excessive soil attached to the roots. The vacuum infiltration was performed with slight modifications to the protocol previously reported.[49,50] The vacuum infiltration was done using a PDS-1000 particle delivery system (Bio-Rad, Hercules, CA, USA). Whole plants were submerged in infiltration mixture containing 3 mL of 5 mM SA solution to a vacuum at ∼25 kPa twice, each for 60 s. Treated plants were then planted in pots. Similarly, raw MSNs and SA@MSN-SS-C10 containing ∼5 mM SA were resuspended in 3 mL of water and vacuum infiltrated into the plants and then planted in pots. Leaf samples were collected at the third, fifth, and seventh day after vacuum infiltration for *PR1* gene expression analysis and GSH quantification.

2.11. Semiquantitative Reverse Transcription Polymerase Chain Reaction. Semiquantitative reverse transcription polymerase chain reaction (RT-PCR) was conducted to test the prolonged up-regulation of *PR1* gene using RNA samples extracted from plants vacuum infiltrated with SA, MSNs, and SA@MSN-SS-C10. For cDNA synthesis, 1 μg of total RNA was isolated using manufacturer's instruction (RNAzol, Molecular Research Center, Cincinnati, OH, USA) to reverse-transcribe in a reaction containing Tetro reverse transcriptase, reaction buffer, and 2 μM random hexamers as per the manufacturer's specifications (Bioline, Alexandria, NSW, Australia). Primers were designed to examine the relative expression of *PR1* and the housekeeping gene actin that was reported being up-regulated post SA treatment. PCR reactions were carried out with GoTaq green master mix and reagents (Promega, Madison, WI, USA). PCR reactions contained 1 μL of cDNA from the RT reaction and 0.5 μM of the appropriate oligonucleotides. PCR cycles consisted of an initial denaturing step of 3 min at 94 °C, followed by repetitions (18−34 cycles, depending on the primer set) of the following three steps: a 30 s denaturation step at 94 °C, 30 s annealing step ranging between 50 and 52 °C, and a 1 min elongation step at 72 °C. Initial reactions were performed to determine the appropriate cycle number for analysis to be conducted within the exponential phase of the PCR reaction (data not shown). PCR products were analyzed on 0.5 × TBE-agarose gels and visualized using ethidium bromide staining. The following primers were used for gene expression analysis of the plant nanoparticle interaction *PR-1* (pathogenesis-related gene 1) 5-AAGAGGCAACTG-CAGACTCA-3′ and 5-TCTCGCTAACCCACATGTTC-3 and actin 5-ACGTGGACATCAGGAAGGAC-3 and 5-GAACCACCGATCCA-GACACT-5. Relative fold change was quantified using ImageJ software program (ImageJ, U.S. National Institutes of Health, Bethesda, MD, USA).

2.12. GSH Quantification Assay. The GSH was measured with the glutathione reductase assay kit using a 96-well plate reader (Sigma). The method relies on the glutathione reductase (GR)-dependent reduction of 5,5-dithiobis-2-nitrobenzoic acid (DTNB), monitored at 412 nm using a spectrophotometer (FluostarOptima, BMG Laboratories). The method measures total glutathione that includes reduced glutathione GSH + GSSG. A fine powder of 50 mg of *Arabidopsis* leaves treated with SA, MSNs, and SA@MSN-SS-C10 was mixed with 1 mL of ice-cold 6% metaphosphoric acid. The suspension was then centrifuged at 14000*g* for 15 min at 4 °C (Eppendorf centrifuge 5804R). The supernatant was collected and kept on ice in

DOI: 10.1021/acsami.5b02131
ACS Appl. Mater. Interfaces 2015, 7, 9937−9946

the dark until use. To measure the total GSH, triplicate aliquots of 10 μL extract were added to plate wells containing appropriate volumes of assay buffer which contains nicotinamide adenine dinucleotide phosphate, DTNB, and GR from the kit, and the total assay volume was calculated to be 220 μL. Standards were run concurrently in the same plates as triplicate assays of 0−50 nmol of GSH in the well. The activity was calculated over 90 s and in all cases was corrected for GSH-independent reduction of DTNB by subtraction of the mean value of triplicate blank assays (0 GSH).

3. RESULTS AND DISCUSSION

3.1. Rationale of Gatekeeping. The main contribution of the current work is to introduce short-chain molecules specifically on the outer surface of MSNs as gatekeepers for controlling the release of loaded biomolecules (Figure 1A). To form disulfide bonds, the thiol groups were first introduced onto the surface of MSNs.

To maintain the pore volume after functionalization, a localized functionalization was applied only onto the outer surface. The as-synthesized MSNs were modified by thiol groups before the CTAB templates were removed. In such a way, the thiol groups were only present on the external surface, while the large pore volume was maintained which benefited

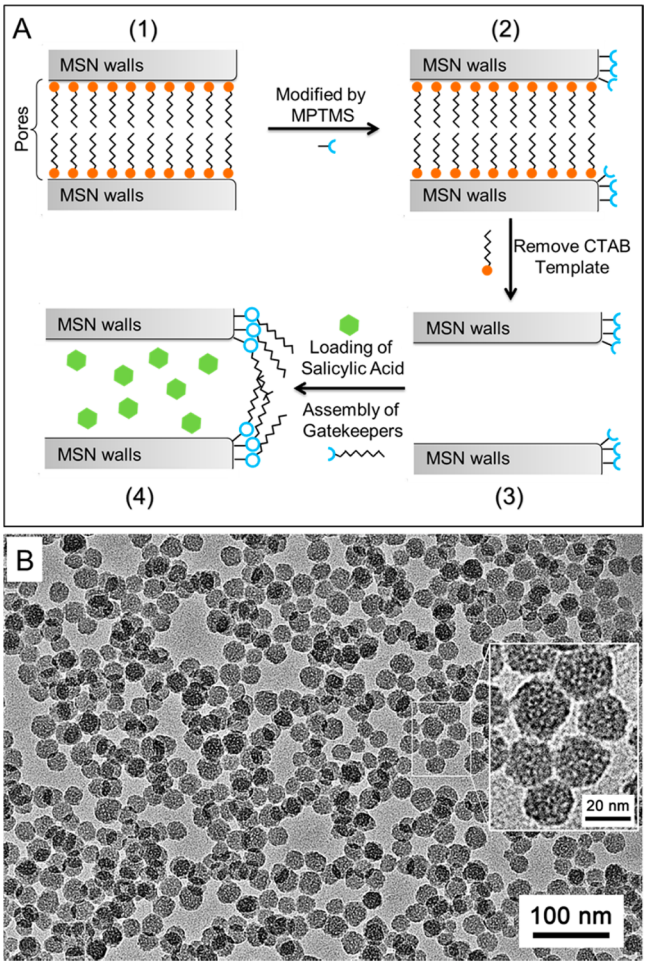

Figure 1. Schematic of functionalization of MSNs with -SH groups and assembly of gatekeepers on to SA-loaded MSNs (A). The localized functionalization of MSNs before removing the template inside the mesopores allows the -SH groups only to graft the entrance of the mesopores. TEM image of MSNs (B). The inset indicates the mesopores (white dots) on MSNs.

the loading of agrochemicals (steps 1 and 2 in Figure 1A). After the thiol groups were grafted on the surface, the CTAB templates were then removed. The mesopores became vacuous for loading agrochemicals (step 3 in Figure 1A).

A gatekeeping strategy was then introduced to prevent the agrochemicals from premature release. The decanethiol, employed as the gatekeepers, are a molecule with thiol terminals which have a short alkyl chain of only about 1.3 nm in length. They not only can block the pore entrance but also have no significant effects on the particle diameter (step 4 in Figure 1A). The disulfide bonds were formed between MSNs and decanethiol and could be cleaved by the endogenous reductants, such as GSH, in plants to release loaded cargos.

Well-dispersed MSNs loaded with biomolecules can be delivered into more tissues, compared to the aggregated MSNs, as has been proved in our previous studies.[12,43] This is because the well-dispersed MSNs offer good permeability through cell membranes[51] and plant cell walls. The spherical and uniformly dispersed MSNs are shown in Figure 1B under TEM and Supporting Information (SI) Figure S1A under SEM. The mesoporous structure of MSNs can be demonstrated from TEM images at a high magnification (inset in Figure 1B). The white dots represent the entrance of the mesopores which shows different contrast from the dark silica framework of the nanoparticles. After the loading of SA and assembling of decanethiol gatekeepers, the particle shape and size were maintained (SI Figure S1A,B).

3.2. Functionalization of MSNs and Assembly of Gatekeepers. The localized functionalization is critical to maintain the particle size and pore volume especially for such small particles with a size of ~20 nm. Before removing CTAB templates, the external surface of as-synthesized MSNs was modified with MPTMS to introduce -SH groups. The successful grafting of -SH groups was determined by Raman spectra (Figure 2A). MSNs possess a characteristic peak at around 800 cm^{-1} that is attributed to the vibration of silanol groups on the surface of silica (Si−OH) and the peak at around 2600 cm^{-1} represents -SH groups in MPTMS. After silanization of MSNs, both Si−OH and -SH can be seen from the Raman spectrum of MSN-SH, which suggests the successful grafting of -SH groups on the surface of MSNs. Due to the introduction of MPTMS, silanol groups of MSNs were consumed, which in turn led to the decrease in their peak intensity at 800 cm^{-1}.

The sulfur in MSN-SH can also be confirmed with SEM-EDS. For a selected region under SEM, elemental mapping was carried out with MSN-SH powder (SI Figure S2A,B). A clear peak at 2.26 keV indicates the sulfur element (SI Figure S2C). The main elemental compositions of MSNs are silicon and oxygen; thus these two elements are evenly spread throughout the whole region and overlapped with each other. However, due to the modification by -SH groups on the outer surface of MSNs, it can be seen from the merged mapping image that the sulfur is sporadically distributed around the selected area (pink dots in SI Figure S2B). These results provide qualitative evidence of the position of -SH on MSNs.

Other evidence to prove the presence of -SH groups on the external surface of MSNs but not the internal surface is from BET results. It can be seen from Table 1 that the surface area of MSN-SH decreases marginally from 363.83 to 346.30 m^2/g and the pore volume decreases from 0.33 to 0.20 cm^3/g. The surface area and pore volume before and after MPTMS modification do not change greatly, which means that the pore area is maintained after functionalization. The -SH groups on

DOI: 10.1021/acsami.5b02131
ACS Appl. Mater. Interfaces 2015, 7, 9937−9946

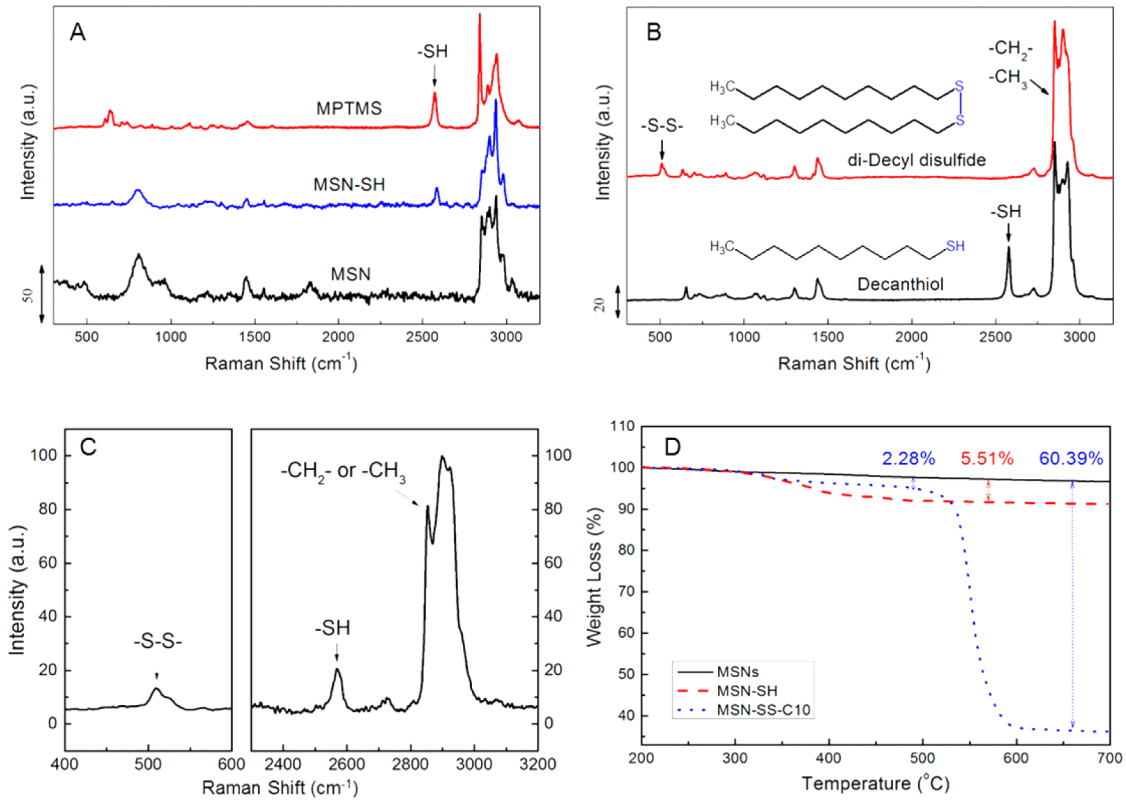

Figure 2. Determination of surface functionalization. (A) Raman spectra of grafting on the surface of MSNs; (B) Raman spectra to determine disulfide formation between decanethiols; (C) Raman spectrum of MSN-SS-C10; and (D) thermogravimetric analysis of nonfunctionalized MSNs and functionalized MSNs (MSN-SH and MSN-SS-C10).

Table 1. BET Surface Areas, Average Pore Sizes, and Pore Volumes of Various MSN Samples Obtained from Nitrogen Sorption Measurement

samples	BET surface area (m^2/g)	av pore size (nm)	pore volume (cm^3/g)
MSNs	363.83 ± 2.22	2.59	0.33
MSN-SH	346.30 ± 1.82	2.22	0.20
SA@MSN	291.49 ± 2.68	3.10	0.21
SA@MSN-SS-C10	85.62 ± 1.43		0.04

the outer surface can be further functionalized to form disulfide bonds, and the retained pore volume provides sufficient space for the effective loading of agrochemicals.

The assembly of decanethiol onto MSNs was conducted through thiol−disulfide exchange. In this reaction, -SH groups are provided by MSN-SH and disulfide bonds are from didecyl disulfide synthesized through a facile oxidation of decanethiol.[47] First, the formation of disulfide bonds between decanethiol molecules were determined by Raman spectroscopy (Figure 2B). It can be seen that the absorption peak at around 2600 cm^{-1} shows the -SH groups in decanethiol molecule[52] and a group of strong absorption peaks between 2800 and 3000 cm^{-1} are the C−H stretching vibration in $-CH_2-$ and $-CH_3$ from the alkyl chain, which are both present in decanethiol and didecyl disulfide. After oxidation, two decanethiol molecules formed one didecyl disulfide. The absorption peak between 500 and 550 cm^{-1} indicates the existence of disulfide bonds.[53,54] Also the peak at around 2600 cm^{-1} disappears, suggesting the complete conversion from thiol to disulfide. After the assembly of decanethiol onto MSN-SH, both -SH groups and disulfide bonds were detected. The thiol groups are revealed at around 2600 cm^{-1}, which indicates the presence of residual -SH groups on nanoparticles (Figure 2C), while disulfide bonds between decanethiol and MSNs lead to the absorption peak at around 500 cm^{-1}. The obvious enhancement of the $-CH_2-/-CH_3$ peak is shown at 2800−3000 cm^{-1}, which is attributed to the introduction of alkyl chain from decanethiol and proves the grafting of decanethiol on MSNs.

To quantify the functional groups on MSNs, the weight loss was measured with thermogravimetric analysis (TGA) when increasing the temperature to 700 °C. All of the functional groups were burnt during this measurement. It can be seen from Figure 2D that MSN-SH and MSN-SS-C10 exhibited a one-step and a two-step decomposition, respectively. The first weight loss of MSN-SS-C10 starts from the same position as MSN-SH does, which means the existence of residual -SH groups on MSNs. The second weight loss starting at around 520 °C illustrates the degradation of disulfide bonds and also alkyl chains from decanethiol. The weight loss caused by -SH groups on MSN-SS-C10 (2.28%) accounts for 41.38% of -SH groups on MSN-SH (5.51%), which means that more than half (58.62%) of the -SH groups on MSN-SH have reacted with didecyl disulfide to form gatekeepers to block guest molecules. The residual -SH groups allow for a fairly slow release of SA from MSN-SS-C10, which benefits the gene expression of plants. It will also be discussed later in the plant section.

3.3. Loading of SA and *in Vitro* Release. Assembly of decanethiol on to MSN-SH was conducted in ethyl acetate which possesses good miscibility with both SA and didecyl disulfide. Through centrifugation, nanoparticles and free SA can be separated. The supernatants were collected to measure the loading efficacy. The standard calibration curves of SA in water

DOI: 10.1021/acsami.5b02131
ACS Appl. Mater. Interfaces 2015, 7, 9937−9946

and ethyl acetate were obtained with different concentrations of SA and linearly fitted. The loading efficacy calculated from UV−vis was 11.71 and 19.38 μg/mg for SA@MSNs and SA@MSN-SS-C10, respectively. The SA loading of decanethiol-capped MSNs is higher than that of MSNs only. Because the particle size was around 20 nm and all of the mesopores were interconnected, the washing procedure could lead to the loss of loaded SA. When decanethiol is incorporated on to MSNs, a higher loading capacity is achieved as the gatekeepers block the loss of SA during the wash. Mesopores were occupied with SA molecules after loading. Nitrogen sorption isotherms of all MSN samples exhibited a similar IV adsorption curve (SI Figure S3A). The decrease in the total absorbed volume of nitrogen at the relative pressure of 0.99 (SI Figure S3B) was proved to be attributed to pore filling of MSNs. In addition, the loading of SA and capping with decanethiol greatly decreased the surface area due to the absorption of SA on the pore and particle surface of the MSNs. SA@MSN-SS-C10 has the lowest surface area (85.62 m^2/g) and pore volume (0.04 cm^3/g), and its average pore size could not be detected due to both the loading of SA and the blocking of pores with decanethiol gatekeepers (Table 1).

The redox-responsive *in vitro* release of SA from MSN-SS-C10 was conducted with different GSH concentrations. The UV−vis spectra of SA, GSH, and their mixture in deionized water were first measured at different time intervals at room temperature (SI Figure S4), to confirm that there was no reaction between SA and GSH. It was found that the calibration peak stays at 296.5 nm without a red or blue shift up to 168 h, which demonstrates that SA maintains stability in GSH solution. This measurement proves the reliability of UV−vis spectra in determining the SA concentration in GSH solution. The *in vitro* release test showed that the release of SA from MSNs was greatly slowed by decanethiol gatekeepers, which is indicated by the release curve of SA@MSN-SS-C10 without GSH (Figure 3A). Only about 5 μg of SA was released from MSN-SS-C10 within 24 h. This is attributed to the residual -SH groups detected by Raman and TG (Figure 2). With the introduction of GSH, however, the release of SA is accelerated. The release reached the plateaus at 800 and 180 min when 5 mM GSH and 10 mM GSH were added, respectively. These results suggest that GSH cleaves the disulfide bonds between decanethiol and MSNs, which allows for the free diffusion of SA from MSNs. The redox-responsive function triggered by GSH has been proved from the release pattern when the GSH was added to the solution. In addition, without gatekeepers, the release of SA from raw MSNs is fairly fast (SA@MSN in Figure 3A). A burst release of SA is detected within 100 min, and then the plateau is achieved. Because there are no gatekeepers for raw MSNs to encapsulate SA, the loaded SA may have been lost during the washing procedure. As a consequence, the released amount when reaching plateaus is also smaller than SA@MSN-SS-C10.

In order to understand the diffusion mechanism of SA from MSNs under different GSH concentrations, the Korsmeyer−Peppas model was employed. This model is to interpret the release kinetics from porous materials:[55]

$$\frac{M_t}{M_\infty} = Kt^n \tag{1}$$

where M_t is the amount of drug released at time t, M_∞ is the amount of drug released at infinite time, K is the release kinetic constant, and n is the release exponent indicating the release mechanism. If taking the logarithm for both sides of eq 1, the following equation is obtained:

$$\log\left(\frac{M_t}{M_\infty}\right) = \log K + n \log t \tag{2}$$

The released data can be fitted by a linear eq 2. If n is less than 0.45, the Fickian mechanism can be applied to the diffusion of SA; if n is between 0.45 and 0.89, then the diffusion follows a non-Fickian mechanism.[55] The initial release stage of SA was selected before 40 min (Figure 3B), because the Korsmeyer−Peppas model is applied to the release percentage less than 60%. The introduction of the gatekeepers changes the mechanism of SA release as shown from the Korsmeyer−Peppas plot (Figure 3C). The release data were fitted by a linear regression, and the obtained n value was listed in SI Table S1. The n value for the sample with 0 mM GSH is 0.76, which indicates that the movement of SA from MSN-SS-C10 is non-Frickian. In another words, SA cannot be freely diffused from MSN-SS-C10 as the chemically bonded decanethiol blocks the diffusion of SA from MSNs. In contrast, with the addition of GSH at the concentrations of 5 and 10 mM, the n values are 0.32 and 0.39, respectively, suggesting that the diffusion of SA is not restricted. The same value of n as 10 mM

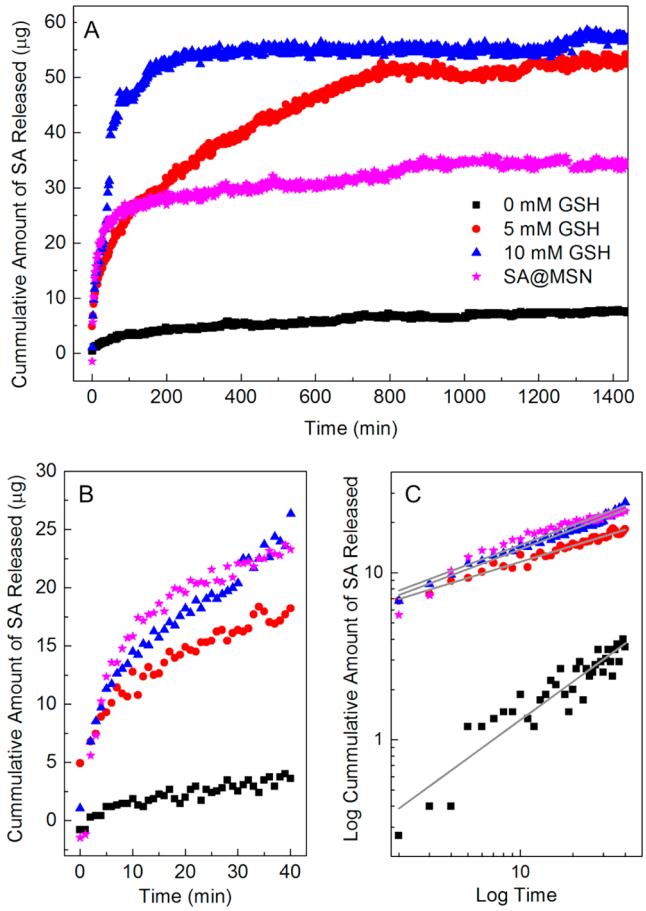

Figure 3. (A) Cumulative amount of SA released from MSN-SS-C10 under different GSH concentrations; (B) release of SA at the initial stage; and (C) logarithmic cumulative amount of SA released versus logarithmic release duration for the sake of fitting with the Korsmeyer−Peppas model at the initial stage. All of the panels use the same symbols that are shown in panel A.

DOI: 10.1021/acsami.5b02131
ACS Appl. Mater. Interfaces 2015, 7, 9937−9946

GSH is shown for the sample of SA@MSN, which means that 10 mM of GSH is high enough to release SA in a way similar to that of MSNs without gatekeepers.

The mechanism of chemical reaction is proposed in Figure 4. For simplicity, only the decanethiol molecules grafted on the edge of the silica wall that have a length of 1.3 nm (Figure 4A) were shown to explain the opening mechanism of the gatekeepers. Decanethiol molecules form a molecular brush at the entrance of mesopores, which blocks SA from being moved around and being released (Figure 4B). After the addition of GSH, the free -SH groups in GSH can cleave disulfide bonds between decanethiol and MSNs. The GSH replaces decanethiol gatekeepers and is covalently bonded to MSNs through disulfide bonds. In this case, the molecular length is shortened from 1.2 nm of the alkane chain in decanethiol to 0.4 nm which is the distance between the main molecular chain and thiol groups in GSH (Figure 4A). This creates a space for the diffusion of SA. In addition, the substituted GSH molecules introduce polar groups such as amine, carboxyl, and amide groups, which have also made a vacancy in the nonpolar network formed by the alkane chains of decanethiol. Due to these two factors, a pathway for the diffusion of SA has been formed between substituted GSH molecules and the original decanethiols (green dashed lines in Figure 4C,D), which allows the release of SA from the inside of the mesopores. The amount of GSH added into this system determines the release rate of SA. When exposed to 5 mM GSH (Figure 4C), the proportion of cleaved disulfide bonds between decanethiol and MSNs was less than that when exposed to 10 mM GSH (Figure 4D). The mesopores were partially blocked at the GSH concentration of 5 mM, while the gatekeepers were completely opened with a higher concentration of GSH (10 mM). Furthermore, the plant cell environment, such as pH which is 5−5.5[56] and various organelles and enzymes, is very complex and the release kinetics can be different from that in pure water. Therefore, *in vitro* experiments would not be able to easily simulate the environment, and the *in vivo* plant test was considered to be the only effective approach to examining the efficacy of gatekeepers in plants. The SA-induced gene expression and GSH accumulation has been investigated and will be discussed in the next section.

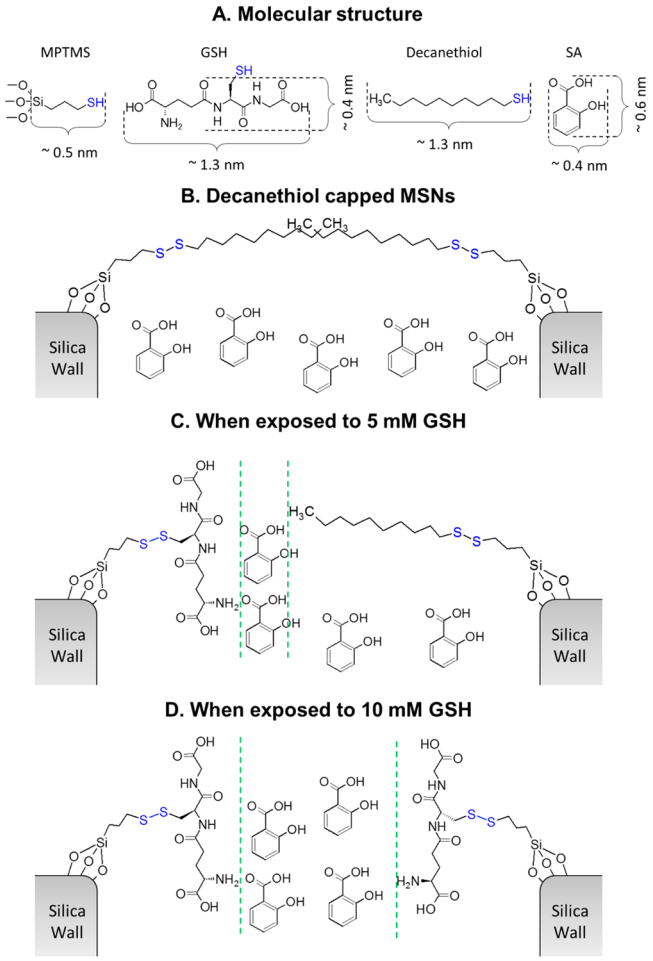

Figure 4. (A) Molecular structure of MPTMS, decanethiol, SA, and GSH. The dimensions of molecules were calculated from Chemsketch software (Advanced Chemistry Development Inc.). Schematic of the chemical reaction during the release of salicylic acid: (B) original structure of decanethiol-capped MSNs loaded with SA without GSH exposure; and cleavage of disulfide bonds between decanethiol and MSNs when exposed to 5 (C) and 10 mM (D) GSH in aqueous solution.

3.4. *PR-1* Gene Expression and GSH Quantification.

Glutathione constitutes one of the major components of the antioxidant defense system and is also the major determinant of the cellular redox status in plants.[57−59] Increased levels of glutathione (GSH) can be detected in plants post exogenous SA treatment, suggesting a physiological coupling between SA and glutathione levels.[60−62] SA mediates plant defenses against biotrophic pathogens, accumulating in both infected and distal leaves in response to pathogen attack. It is well-established that various pathogenesis-related genes and defense compounds are induced in response to SA.[63,64] In *Arabidopsis*, exogenous application of SA is capable of providing resistance to a variety of pathogens and has been widely reported.[65] Despite its importance in plant defense against pathogens, the longevity and its effect on pathogenesis-related gene expression is short-lived.[66−68]

The effect of SA@MSN-SS-C10 on the controlled release of SA in *Arabidopsis* was examined and tested through the expression of *PR-1*, a SA inducible marker gene along with the level of GSH accumulation. The *PR-1* defense gene and total enzymatic activity of GSH was measured at different days (3, 5, and 7) post vacuum infiltration with MSNs, free SA, and SA@MSN-SS-C10. For the plants without any treatment, there is no *PR-1* expression at these days (SI Figure S5), while a slight increase in *PR-1* gene expression was observed at day 3 when plants were exposed to MSNs (Figure 5A). This effect was likely a result of mechanical wounding[69] caused by the vacuum infiltration. As expected, no *PR-1* gene expression could be detected in plants treated with MSNs alone at days 5 and 7 (Figure 5A). However, when plants were treated with free SA (5 mM), *PR-1* gene expression was highly expressed at day 3, but started to decline at day 5, and could not be detected at day 7 (Figure 5A). The reduction in the *PR-1* across the time course is consistent with other reports.[70] Most interestingly, it was found that when *Arabidopsis* were treated with SA@MSN-SS-C10, *PR-1* expression could be detected across all of the days tested (Figure 5A), an effect of a constant supply of SA released from the pores of the MSNs. The representative photos of *Arabidopsis* seedlings were taken at day 7 and showed in SI Figure S6. During the 7 day testing, the treatments of plants with nanoparticles have no significant impact on the growth and development of plant seedlings.

DOI: 10.1021/acsami.5b02131
ACS Appl. Mater. Interfaces 2015, 7, 9937−9946

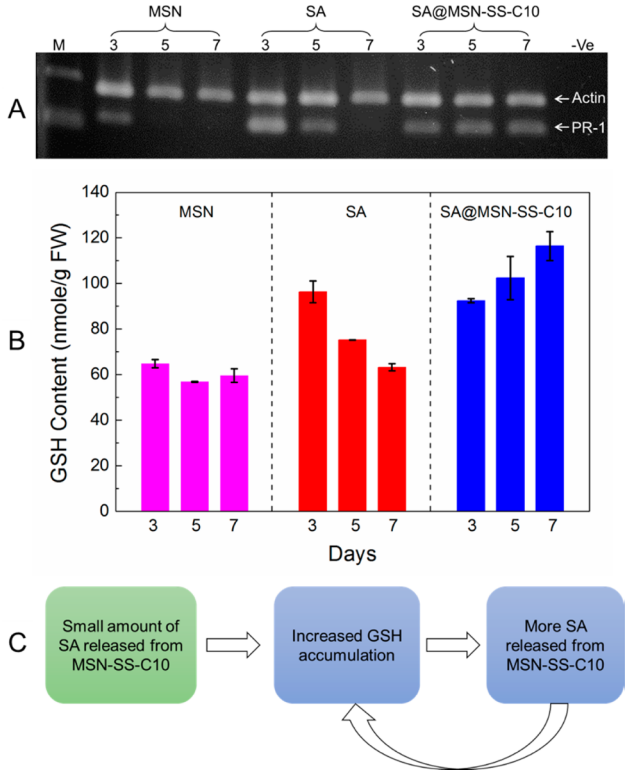

Figure 5. (A) Housekeeping gene actin and defense gene (*PR-1*) expression in *Arabidopsis* with MSN, SA, and SA@MSN-SS-C10 treatment on days 3, 5, and 7. M is HyperLadder IV (Bioline) and -Ve is the blank channel. Actin is at the top row, and *PR-1* is at the bottom row. (B) GSH accumulation in *Arabidopsis* leaves post vacuum infiltration with MSN, SA, and SA@MSN-SS-C10. The values for each data point represent the mean ± SE of three replicates. FW, fresh weight. (C) Schematic of the relationship between SA release and GSH accumulation.

The controlled release of SA under *in vitro* conditions was tested and confirmed prior to exposing SA@MSN-SS-C10 to *Arabidopsis* (Figure 3A). To show there is a physiological coupling between SA and GSH levels in plants, the accumulation of GSH in plants was also quantified. It was found that when plants were exposed to free SA, an enhanced pool of GSH was observed at day 3 which had returned to levels found with MSNs by day 7 (Figure 5C). Most interestingly, when *Arabidopsis* were exposed to SA@MSN-SS-C10, constant accumulation of GSH was observed for all of the days tested. Together, *PR-1* gene expression levels and GSH quantification indicate that SA@MSN-SS-C10 provides a sustained release of SA to plants that could provide prolonged protection against biotic stress.

4. CONCLUSIONS

The concept of using short-chain molecules as gatekeepers to encapsulate biomolecules in MSNs was proved, and the controlled release of SA from gatekeeper-capped MSNs was investigated *in vitro* and *in vivo*. The microscopic and spectroscopic characterizations were employed to confirm the successful assembly of decanethiols on MSNs. The *in vitro* release measurement suggested that decanethiol gatekeepers can decrease the release rate of SA with the absence of GSH. The introduction of GSH (5 and 10 mM) cleaved the disulfide bonds between decanethiol and MSNs and opened the gatekeeper, accelerating the release of SA. The higher the concentration (10 mM), the faster the release. With the help of redox-stimuli release mechanism, smart release of agrochemicals can be achieved. Preliminary *in planta* experiments showed that the plant pathogen defense gene (*PR-1*) can be expressed at a high level for up to 7 days in *Arabidopsis* treated with SA-loaded and decanethiol-capped MSNs, and the accumulation of GSH in plants was also found to be associated with SA release from MSNs. The use of MSNs with redox-responsive gatekeepers has been proved in this study to be a potential and efficient technique to deliver agrochemicals into plants in a controllable fashion. Future work will focus on the effectiveness of this agrochemical delivery system in crop plants (maize, soybean, and wheat, etc.) and the corresponding assay of plant pathogen resistance.

■ ASSOCIATED CONTENT

Ⓢ Supporting Information

Figures showing SEM images of MSNs before and after SA loading and assembling of decanethiol gatekeepers, SEM-EDS analysis of thiol groups on MSN-SH, nitrogen sorption isotherms of MSN samples, evidence of no reaction between SA and GSH, *PR-1* gene expression in the plants without any treatment, and representative photographs of *Arabidopsis* seedlings post nanoparticle treatment at day 7 and a table of fitting results for release kinetics. The Supporting Information is available free of charge on the ACS Publications website at DOI: 10.1021/acsami.5b02131.

■ AUTHOR INFORMATION

Corresponding Authors

*(L.K.) E-mail: lingxue.kong@deakin.edu.au.
*(D.M.C.) E-mail: david.cahill@deakin.edu.au.

Notes

The authors declare no competing financial interest.

■ ACKNOWLEDGMENTS

We acknowledge Deakin University for providing scholarships. We thank Leonora Velleman at the Institute for Frontier Materials, Deakin University for helping with the work on online detection of SA release on UV−vis spectroscopy and Andrew Sullivan and Rosey Van Driel at the Institute for Frontier Materials, Deakin University for their help with electron microscopy. We thank Chengpeng Li at the Institute for Frontier Materials, Deakin University for a comprehensive discussion on chemical reaction.

■ REFERENCES

(1) Wu, S.-H.; Mou, C.-Y.; Lin, H.-P. Synthesis of Mesoporous Silica Nanoparticles. *Chem. Soc. Rev.* **2013**, *42* (9), 3862−3875.
(2) Slowing, I. I.; Vivero-Escoto, J. L.; Wu, C.-W.; Lin, V. S. Y. Mesoporous Silica Nanoparticles as Controlled Release Drug Delivery and Gene Transfection Carriers. *Adv. Drug Delivery Rev.* **2008**, *60* (11), 1278−1288.
(3) Yamada, H.; Urata, C.; Ujiie, H.; Yamauchi, Y.; Kuroda, K. Preparation of Aqueous Colloidal Mesostructured and Mesoporous Silica Nanoparticles with Controlled Particle Size in a Very Wide Range from 20 to 700 nm. *Nanoscale* **2013**, *5* (13), 6145−6153.
(4) Yu, M.; Zhou, L.; Zhang, J.; Yuan, P.; Thorn, P.; Gu, W.; Yu, C. A Simple Approach to Prepare Monodisperse Mesoporous Silica Nanospheres with Adjustable Sizes. *J. Colloid Interface Sci.* **2012**, *376* (1), 67−75.
(5) Xu, H.; Li, Y.; Yang, Z.; Ding, Y.; Lu, C.; Li, D.; Xu, Z. Preparation of Monodispersed Mesoporous Silica Spheres with

DOI: 10.1021/acsami.5b02131
ACS Appl. Mater. Interfaces 2015, 7, 9937−9946

Controllable Particle Size under an Alkaline Condition. *Int. J. Appl. Ceram. Technol.* **2012**, *9* (6), 1112−1123.
(6) Na, H.-K.; Kim, M.-H.; Park, K.; Ryoo, S.-R.; Lee, K. E.; Jeon, H.; Ryoo, R.; Hyeon, C.; Min, D.-H. Efficient Functional Delivery of siRNA using Mesoporous Silica Nanoparticles with Ultralarge Pores. *Small* **2012**, *8* (11), 1752−1761.
(7) Kobler, J.; Möller, K.; Bein, T. Colloidal Suspensions of Functionalized Mesoporous Silica Nanoparticles. *ACS Nano* **2008**, *2* (4), 791−799.
(8) Yang, H.; Zheng, K.; Zhang, Z.; Shi, W.; Jing, S.; Wang, L.; Zheng, W.; Zhao, D.; Xu, J.; Zhang, P. Adsorption and Protection of Plasmid DNA on Mesoporous Silica Nanoparticles Modified with Various Amounts of Organosilane. *J. Colloid Interface Sci.* **2012**, *369* (1), 317−322.
(9) Kim, T.-W.; Slowing, I. I.; Chung, P.-W.; Lin, V. S.-Y. Ordered Mesoporous Polymer−Silica Hybrid Nanoparticles as Vehicles for the Intracellular Controlled Release of Macromolecules. *ACS Nano* **2010**, *5* (1), 360−366.
(10) Mahony, D.; Cavallaro, A. S.; Stahr, F.; Mahony, T. J.; Qiao, S. Z.; Mitter, N. Mesoporous Silica Nanoparticles Act as a Self-Adjuvant for Ovalbumin Model Antigen in Mice. *Small* **2013**, *9* (18), 3138−3146.
(11) Tang, F.; Li, L.; Chen, D. Mesoporous Silica Nanoparticles: Synthesis, Biocompatibility and Drug Delivery. *Adv. Mater.* **2012**, *24* (12), 1504−1534.
(12) Hussain, H.; Yi, Z.; Rookes, J.; Kong, L.; Cahill, D. Mesoporous Silica Nanoparticles as A Biomolecule Delivery Vehicle in Plants. *J. Nanopart. Res.* **2013**, *15* (6), 1676−1690.
(13) Napierska, D.; Thomassen, L. C. J.; Lison, D.; Martens, J. A.; Hoet, P. H. The Nanosilica Hazard: Another Variable Entity. *Part. Fibre Toxicol.* **2010**, *7* (1), 39.
(14) Prow, T. W.; Grice, J. E.; Lin, L. L.; Faye, R.; Butler, M.; Becker, W.; Wurm, E. M. T.; Yoong, C.; Robertson, T. A.; Soyer, H. P.; Roberts, M. S. Nanoparticles and Microparticles for Skin Drug Delivery. *Adv. Drug Delivery Rev.* **2011**, *63* (6), 470−491.
(15) Niu, D.; Liu, Z.; Li, Y.; Luo, X.; Zhang, J.; Gong, J.; Shi, J. Monodispersed and Ordered Large-Pore Mesoporous Silica Nanospheres with Tunable Pore Structure for Magnetic Functionalization and Gene Delivery. *Adv. Mater.* **2014**, *26* (29), 4947−4953.
(16) Li, Y.; Shi, J. Hollow-Structured Mesoporous Materials: Chemical Synthesis, Functionalization and Applications. *Adv. Mater.* **2014**, *26* (20), 3176−3205.
(17) Martin-Ortigosa, S.; Valenstein, J. S.; Lin, V. S. Y.; Trewyn, B. G.; Wang, K. Gold Functionalized Mesoporous Silica Nanoparticle Mediated Protein and DNA Codelivery to Plant Cells Via the Biolistic Method. *Adv. Funct. Mater.* **2012**, *22* (17), 3576−3582.
(18) Martin-Ortigosa, S.; Peterson, D. J.; Valenstein, J. S.; Lin, V. S. Y.; Trewyn, B. G.; Lyznik, L. A.; Wang, K. Mesoporous Silica Nanoparticle-Mediated Intracellular cre Protein Delivery for Maize Genome Editing via loxP Site Excision. *Plant Physiol.* **2014**, *2*, 537.
(19) Torney, F.; Trewyn, B. G.; Lin, V. S. Y.; Wang, K. Mesoporous Silica Nanoparticles Deliver DNA and Chemicals into Plants. *Nat. Nanotechnol.* **2007**, *2* (5), 295−300.
(20) Yang, Y.-J.; Tao, X.; Hou, Q.; Ma, Y.; Chen, X.-L.; Chen, J.-F. Mesoporous Silica Nanotubes Coated with Multilayered Polyelectrolytes for pH-Controlled Drug Release. *Acta Biomater.* **2010**, *6* (8), 3092−3100.
(21) Liu, R.; Zhang, Y.; Zhao, X.; Agarwal, A.; Mueller, L. J.; Feng, P. pH-Responsive Nanogated Ensemble Based on Gold-Capped Mesoporous Silica through an Acid-Labile Acetal Linker. *J. Am. Chem. Soc.* **2010**, *132* (5), 1500−1501.
(22) Muhammad, F.; Guo, M.; Qi, W.; Sun, F.; Wang, A.; Guo, Y.; Zhu, G. pH-Triggered Controlled Drug Release from Mesoporous Silica Nanoparticles via Intracelluar Dissolution of ZnO Nanolids. *J. Am. Chem. Soc.* **2011**, *133* (23), 8778−8781.
(23) Yuan, L.; Tang, Q.; Yang, D.; Zhang, J. Z.; Zhang, F.; Hu, J. Preparation of pH-Responsive Mesoporous Silica Nanoparticles and Their Application in Controlled Drug Delivery. *J. Phys. Chem. C* **2011**, *115* (20), 9926−9932.
(24) Ye, F.; Qin, J.; Toprak, M.; Muhammed, M. Multifunctional Core−Shell Nanoparticles: Superparamagnetic, Mesoporous, and Thermosensitive. *J. Nanopart. Res.* **2011**, *13* (11), 6157−6167.
(25) Niu, N.; He, F.; Ma, P. a.; Gai, S.; Yang, G.; Qu, F.; Wang, Y.; Xu, J.; Yang, P. Up-Conversion Nanoparticle Assembled Mesoporous Silica Composites: Synthesis, Plasmon-Enhanced Luminescence, and Near-Infrared Light Triggered Drug Release. *ACS Appl. Mater. Interfaces* **2014**, *6* (5), 3250−3262.
(26) Li, H.; Tan, L.-L.; Jia, P.; Li, Q.-L.; Sun, Y.-L.; Zhang, J.; Ning, Y.-Q.; Yu, J.; Yang, Y.-W. Near-Infrared Light-Responsive Supramolecular Nanovalve Based on Mesoporous Silica-Coated Gold Nanorods. *Chem. Sci.* **2014**, *5* (7), 2804−2808.
(27) Zhang, Z.; Wang, L.; Wang, J.; Jiang, X.; Li, X.; Hu, Z.; Ji, Y.; Wu, X.; Chen, C. Mesoporous Silica-Coated Gold Nanorods as a Light-Mediated Multifunctional Theranostic Platform for Cancer Treatment. *Adv. Mater.* **2012**, *24* (11), 1418−1423.
(28) Koo, A.; Rim, H.; Park, D.; Kim, J.-H.; Jeong, S.; Lee, S. Glutathione-Mediated Intracellular Release of Anti-inflammatory *N*-acetyl-L-Cysteine from Mesoporous Silica Nanoparticles. *Macromol. Res.* **2013**, *21* (7), 809−814.
(29) Cui, Y.; Dong, H.; Cai, X.; Wang, D.; Li, Y. Mesoporous Silica Nanoparticles Capped with Disulfide-Linked PEG Gatekeepers for Glutathione-Mediated Controlled Release. *ACS Appl. Mater. Interfaces* **2012**, *4* (6), 3177−3183.
(30) Kim, H.; Kim, S.; Park, C.; Lee, H.; Park, H. J.; Kim, C. Glutathione-Induced Intracellular Release of Guests from Mesoporous Silica Nanocontainers with Cyclodextrin Gatekeepers. *Adv. Mater.* **2010**, *22* (38), 4280−4283.
(31) Lai, C.-Y.; Trewyn, B. G.; Jeftinija, D. M.; Jeftinija, K.; Xu, S.; Jeftinija, S.; Lin, V. S. Y. A Mesoporous Silica Nanosphere-Based Carrier System with Chemically Removable CdS Nanoparticle Caps for Stimuli-Responsive Controlled Release of Neurotransmitters and Drug Molecules. *J. Am. Chem. Soc.* **2003**, *125* (15), 4451−4459.
(32) Giri, S.; Trewyn, B. G.; Stellmaker, M. P.; Lin, V. S. Y. Stimuli-Responsive Controlled-Release Delivery System Based on Mesoporous Silica Nanorods Capped with Magnetic Nanoparticles. *Angew. Chem., Int. Ed.* **2005**, *44* (32), 5038−5044.
(33) Zhang, Q.; Liu, F.; Nguyen, K. T.; Ma, X.; Wang, X.; Xing, B.; Zhao, Y. Multifunctional Mesoporous Silica Nanoparticles for Cancer-Targeted and Controlled Drug Delivery. *Adv. Funct. Mater.* **2012**, *22* (24), 5144−5156.
(34) Dietz, K.-J.; Herth, S. Plant Nanotoxicology. *Trends Plant Sci.* **2011**, *16* (11), 582−589.
(35) Szejtli, J. Physiological Effects of Cyclodextrins on Plants. *Starch/Stärke* **1983**, *35* (12), 433−438.
(36) Wanyika, H.; Gatebe, E.; Kioni, P.; Tang, Z.; Gao, Y. Mesoporous Silica Nanoparticles Carrier for Urea: Potential Applications in Agrochemical Delivery Systems. *J. Nanosci. Nanotechnol.* **2012**, *12* (3), 2221−2228.
(37) Fleischer, A.; O'Neill, M. A.; Ehwald, R. The Pore Size of Non-Graminaceous Plant Cell Walls Is Rapidly Decreased by Borate Ester Cross-Linking of the Pectic Polysaccharide Rhamnogalacturonan II. *Plant Physiol.* **1999**, *121* (3), 829−838.
(38) Rondeau-Mouro, C.; Defer, D.; Leboeuf, E.; Lahaye, M. Assessment of Cell Wall Porosity in Arabidopsis Thaliana by NMR Spectroscopy. *Int. J. Biol. Macromol.* **2008**, *42* (2), 83−92.
(39) Tepfer, M.; Taylor, I. E. P. The Permeability of Plant Cell Walls as Measured by Gel Filtration Chromatography. *Science* **1981**, *213* (4509), 761−763.
(40) Carpita, N.; Sabularse, D.; Montezinos, D.; Delmer, D. P. Determination of the Pore Size of Cell Walls of Living Plant Cells. *Science* **1979**, *205* (4411), 1144−1147.
(41) Adani, F.; Papa, G.; Schievano, A.; Cardinale, G.; D'Imporzano, G.; Tambone, F. Nanoscale Structure of the Cell Wall Protecting Cellulose from Enzyme Attack. *Environ. Sci. Technol.* **2010**, *45* (3), 1107−1113.
(42) Chang, F.-P.; Kuang, L.-Y.; Huang, C.-A.; Jane, W.-N.; Hung, Y.; Hsing, Y.-i. C.; Mou, C.-Y. A Simple Plant Gene Delivery System

DOI: 10.1021/acsami.5b02131
ACS Appl. Mater. Interfaces 2015, 7, 9937−9946

Using Mesoporous Silica Nanoparticles as Carriers. *J. Mater. Chem. B* **2013**, *1* (39), 5279−5287.
(43) Sun, D.; Hussain, H. I.; Yi, Z.; Siegele, R.; Cresswell, T.; Kong, L.; Cahill, D. M. Uptake and Cellular Distribution, in Four Plant Species, of Fluorescently Labeled Mesoporous Silica Nanoparticles. *Plant Cell Rep.* **2014**, *33* (8), 1389−1402.
(44) Liu, C.; Wang, X.; Lee, S.; Pfefferle, L. D.; Haller, G. L. Surfactant Chain Length Effect on the Hexagonal-to-Cubic Phase Transition in Mesoporous Silica Synthesis. *Microporous Mesoporous Mater.* **2012**, *147* (1), 242−251.
(45) Nooney, R. I.; Thirunavukkarasu, D.; Chen, Y.; Josephs, R.; Ostafin, A. E. Synthesis of Nanoscale Mesoporous Silica Spheres with Controlled Particle Size. *Chem. Mater.* **2002**, *14* (11), 4721−4728.
(46) He, Q.; Cui, X.; Cui, F.; Guo, L.; Shi, J. Size-Controlled Synthesis of Monodispersed Mesoporous Silica Nano-Spheres under A Neutral Condition. *Microporous Mesoporous Mater.* **2009**, *117* (3), 609−616.
(47) Kirihara, M.; Asai, Y.; Ogawa, S.; Noguchi, T.; Hatano, A.; Hirai, Y. A Mild and Environmentally Benign Oxidation of Thiols to Disulfides. *ChemInform* **2008**, *39* (12), 3286−3289.
(48) Foster, R.; Chua, N.-H. An Arabidopsis Mutant with Deregulated ABA Gene Expression: Implications for Negative Regulator Function. *Plant J.* **1999**, *17* (4), 363−372.
(49) Tian, J.; Pei, H.; Zhang, S.; Chen, J.; Chen, W.; Yang, R.; Meng, Y.; You, J.; Gao, J.; Ma, N. TRV-GFP: A Modified Tobacco Rattle Virus Vector for Efficient and Visualizable Analysis of Gene Function. *J. Exp. Bot.* **2014**, *65* (1), 311−322.
(50) Marion, J.; Bach, L.; Bellec, Y.; Meyer, C.; Gissot, L.; Faure, J. D. Systematic Analysis of Protein Subcellular Localization and Interaction Using High-Throughput Transient Transformation of Arabidopsis Seedlings. *Plant J.* **2008**, *56* (1), 169−79.
(51) Guan, B.; Cui, Y.; Ren, Z.; Qiao, Z.-a.; Wang, L.; Liu, Y.; Huo, Q. Highly Ordered Periodic Mesoporous Organosilica Nanoparticles with Controllable Pore Structures. *Nanoscale* **2012**, *4* (20), 6588−6596.
(52) Velleman, L.; Bruneel, J.-L.; Guillaume, F.; Losic, D.; Shapter, J. G. Raman Spectroscopy Probing of Self-Assembled Monolayers Inside the Pores of Gold Nanotube Membranes. *Phys. Chem. Chem. Phys.* **2011**, *13* (43), 19587−19593.
(53) Van Wart, H. E.; Scheraga, H. A. Raman Spectra of Strained Disulfides. Effect of Rotation about Sulfur-Sulfur Bonds on Sulfur-Sulfur Stretching Frequencies. *J. Phys. Chem.* **1976**, *80* (16), 1823−1832.
(54) Gosselin, M.-È.; Kapustij, C. J.; Venkateswaran, U. D.; Leverenz, V. R.; Giblin, F. J. Raman Spectroscopic Evidence for Nuclear Disulfide in Isolated Lenses of Hyperbaric Oxygen-Treated Guinea Pigs. *Exp. Eye Res.* **2007**, *84* (3), 493−499.
(55) Korsmeyer, R. W.; Gurny, R.; Doelker, E.; Buri, P.; Peppas, N. A. Mechanisms of Solute Release from Porous Hydrophilic Polymers. *Int. J. Pharm.* **1983**, *15* (1), 25−35.
(56) Rost, T. L.; Barbour, M. G.; Stocking, C. R.; Murphy, T. M. *Plant Biology*; Thomson Higher Education: Belmont, CA, USA, 2006.
(57) Blokhina, O.; Virolainen, E.; Fagerstedt, K. V. Antioxidants, Oxidative Damage and Oxygen Deprivation Stress: A Review. *Ann. Bot.* **2003**, *91* (2), 179−194.
(58) Foyer, C. H.; Noctor, G. Redox Homeostasis and Antioxidant Signaling: A Metabolic Interface between Stress Perception and Physiological Responses. *Plant Cell* **2005**, *17* (7), 1866−1875.
(59) Mullineaux, P.; Rausch, T. Glutathione, Photosynthesis and the Redox Regulation of Stress-Responsive Gene Expression. *Photosynth. Res.* **2005**, *86* (3), 459−474.
(60) Peterson, L. C.; Haug, G. H.; Hughen, K. A.; Röhl, U. Rapid Changes in the Hydrologic Cycle of the Tropical Atlantic During the Last Glacial. *Science* **2000**, *290* (5498), 1947−1951.
(61) Freeman, J. L.; Garcia, D.; Kim, D. G.; Hopf, A.; Salt, D. E. Constitutively Elevated Salicylic Acid Signals Glutathione-Mediated Nickel Tolerance in Thlaspi Nickel Hyperaccumulators. *Plant Physiol.* **2005**, *137* (3), 1082−1091.
(62) Mateo, A.; Funck, D.; Muhlenbock, P.; Kular, B.; Mullineaux, P. M.; Karpinski, S. Controlled Levels of Salicylic Acid are Required for Optimal Photosynthesis and Redox Homeostasis. *J. Exp. Bot.* **2006**, *57* (8), 1795−1807.
(63) Glazebrook, J. Contrasting Mechanisms of Defense Against Biotrophic and Necrotrophic Pathogens. *Annu. Rev. Phytopathol.* **2005**, 205−227.
(64) Wildermuth, M. C.; Dewdney, J.; Wu, G.; Ausubel, F. M. Isochorismate Synthase is Required to Synthesize Salicylic Acid for Plant Defence. *Nature* **2001**, *414* (6863), 562−565.
(65) Donald, E. C.; Porter, I. J. Clubroot in Australia: The History and Impact of *Plasmodiophora brassicae* in *Brassica* Crops and Research Efforts Directed Towards its Control. *Can. J. Plant Pathol.* **2014**, *36*, 66−84 (Special Issue).
(66) Vlot, A. C.; Dempsey, D. M. A.; Klessig, D. F. Salicylic Acid, a Multifaceted Hormone to Combat Disease. *Annu. Rev. Phytopathol.* **2009**, 177−206.
(67) Fariduddin, Q.; Hayat, S.; Ahmad, A. Salicylic Acid Influences Net Photosynthetic Rate, Carboxylation Efficiency, Nitrate Reductase Activity, and Seed Yield in Brassica Juncea. *Photosynthetica* **2003**, *41* (2), 281−284.
(68) Rivas-San Vicente, M.; Plasencia, J. Salicylic Acid Beyond Defence: Its Role in Plant Growth and Development. *J. Exp. Bot.* **2011**, *62* (10), 3321−3338.
(69) Reymond, P.; Weber, H.; Damond, M.; Farmer, E. E. Differential Gene Expression in Response to Mechanical Wounding and Insect Feeding in Arabidopsis. *Plant Cell* **2000**, *12* (5), 707−719.
(70) Van Wees, S. C. M.; Glazebrook, J. Loss of Non-host Resistance of Arabidopsis NahG to Pseudomonas Syringae pv. Phaseolicola Is due to Degradation Products of Salicylic Acid. *Plant J.* **2003**, *33* (4), 733−742.

DOI: 10.1021/acsami.5b02131
ACS Appl. Mater. Interfaces 2015, 7, 9937−9946